ASTEROID MAGNETIZATION BY THE EARLY SOLAR WIND. A. Anand[1], J. Carroll-Nellenback[1,2], E.G. Blackman[1,2] and J.A. Tarduno[1,2,3], [1]Department of Physics & Astronomy, University of Rochester, Rochester, NY 14627 (aanand6@ur.rochester.edu), [2]Laboratory for Laser Energetics, University of Rochester, Rochester, NY 14623, [3]Department of Earth & Environmental Science, University of Rochester, Rochester, NY 14627.

Introduction: Magnetic fields provide an important probe of the thermal, material, and structural history of planetary and sub-planetary bodies. Core dynamos are a potential source of magnetic fields for differentiated bodies, but evidence for magnetization in undifferentiated bodies requires a different mechanism, external to the body. It is often unclear whether smaller rocky Solar System bodies like asteroids experienced sufficient differentiation to generate a liquid core. The CV3 meterorite Allende, long thought to be from an undifferentiated body [1], has a relatively high bulk magnetization but only recently has this been interpreted to require a core dynamo, and hence differentiation [2]. However, no other evidence for Allende's differentiation exists. More recently it was discovered [3] that Allende's magnetization is a consequence of magnetic interactions associated with its magnetic mineralogy, especially pyrrhotite, rather than a reliable paleofield recorder, voiding the need for parent body differentiation, and excluding the reliable recording of a nebular field [4]. Fortunately, other CV (e.g., CV3 meteorite Kaba) and CM (Mighei-type) carbonaceous chondrites meteorites have higher fidelity magnetic recorders (i.e., magnetite), which yield paleofield strength values of $\sim 1\mu T$ [5]. The actual magnetization of these meteorites will depend on when and how long magnetite passed through relevant blocking temperatures imparting thermoremanent magnetizations or grew through blocking volumes, imparting chemical remanent magnetizations. Solar wind induced magnetization is one external mechanism to explain the magnetization of these, and other meteorites from undifferentiated parent bodies [6].

We studied [3,7] the amplified field provided by the stellar wind to an initially unmagnetized body using analytic theory and numerical simulations, employing the resistive MHD AstroBEAR [8-9] adaptive mesh refinement (AMR) multiphysics code. We obtain a broadly applicable scaling relation for the peak magnetization achieved once a wind advects, piles-up, and drapes a body with magnetic field, reaching a quasi-steady state. We find that the dayside magnetic field for a sufficiently conductive body saturates when it balances the sum of incoming solar wind ram, magnetic, and thermal pressures. Stronger amplification results from pileup by denser, faster, and more magnetic winds.

Methods: The early solar wind is thought to have a higher density and magnetic field strength than that of the present day [10-12]. We assign the young stellar wind an ion density of 300 cm^{-3} or 1000 cm^{-3} (Wind I or Wind II), a temperature of 5×10^5 K, a velocity of 500 km s^{-1} (in x), and a magnetic field of 100 nT (in the y direction) perpendicular to the flow. The above values correspond to a stellar wind Mach number (M) of 4.74, the ratio of thermal to magnetic pressure (β) of 1.04 or 3.47, and an Alfvenic Mach number of 4.38 or 8. We use a separate wind (Wind III) having parameters of 300 cm^{-3}, 150×10^3 K, 500 km s^{-1}, and 14 nT to test the effects of our grid (see [7], Table 1 for more details). The mean mass of solar wind particles in all cases is 0.623 amu.

This wind overruns an asteroid modelled as a partially absorbing internal boundary of radius 500 km, which can have a spatially varying internal resistivity. The resistivity profiles used presently are 1. constant (e.g. small asteroids); 2. shell-like (e.g. small bodies with an atmosphere), with the outer 10% radius having 10x the conductivity of the internal body; and 3. cometary, with the day side of the outer 10% radius having 10x the conductivity of the rest of the asteroid.

The finite element method (FEM) analysis of the resistive magnetic induction equation in AstroBEAR allows us to find the equivalent resistivity of a mixture of minerals. This is being adapted to estimate the internal resistivity structure of (16) Psyche [13]. The resistivity of the body is converted to the dimensionless magnetic Reynolds' number, $R_M \equiv \frac{2v_w R}{\bar{\eta}}$ for ease of quantification. Here, $\bar{\eta}$ is the equivalent magnetic diffusivity, v_w is the wind velocity, and R is the radius of the body. The body conductivity is weighed by current and inverted to obtain $\bar{\eta}$. For numerical diffusion of scale parameter α, numerical magnetic Reynolds' number $R_{M\alpha}$, and specific heat ratio $\gamma(=5/3)$, the maximum theoretical amplification, A, is given by:

$$A = \max\left[1, \min\left(M\sqrt{\gamma\beta}, R_M, R_{M\alpha}\right)\right] \qquad (1)$$

Results: A suite of runs were carried out to sweep the parameter space for the 3 resistivity profiles. A summary of results is shown in Figure 1. Figure 2 shows select steady state parameters for Wind II incident on body with constant $R_M = 5{,}000$. Equation 1 represents the overall trend, with the minimum amplification being 1, rising linearly with R_M, and saturating at $M\sqrt{\gamma\beta}$. However, it overpredicts the magnetic amplification for cases with higher β (denser wind, Wind II in red in Figure 1), suggesting that thermal pressure contributes to total pressure, thereby reducing magnetic pressure needed to balance ram pressure. Profiles having an outer conductive 10% shell, as in our cometary and shell

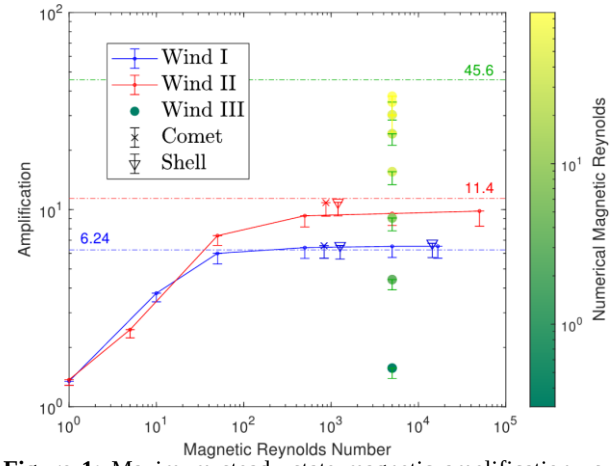

Figure 1: Maximum steady state magnetic amplification vs magnetic Reynolds number for simulations with three solar wind models (from [10]). Solid curves: constant resistivity with different R_M but constant $R_{M\alpha} = 44$. Filled circles: Wind III case with fill color giving $R_{M\alpha}$. Crosses: shell. Down triangles: cometary. Dotted lines: wind $M\sqrt{\gamma\beta}$ (see Equation 1). High values of error bars correspond to global maxima at the dayside of the body directly perpendicular to the wind, while low values are the L16 norm over a R/2 (250 km) region around it.

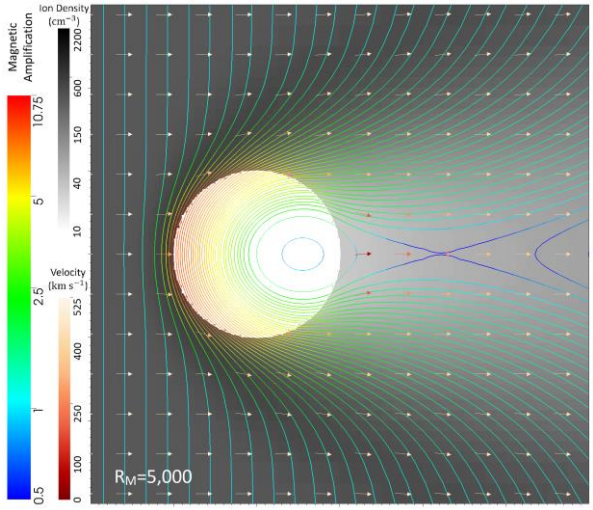

Figure 2: Steady state magnetic amplification lines, ion density, and wind velocity (*xy* mid-plane) for Wind II model with constant resistivity profile with R_M = 5,000. The velocity scale is linear while others are logscale (Fig. 3f in [10])].

models, have higher pileups than cases with the same effective conductivity but distributed uniformly. But this high field is at the outer boundary of the shell (due to higher gradients) and can reach the main body only after atmospheric turbulent mixing. Cometary cases differ from shell cases by having slightly lower amplification and no "kinks" in the magnetic field on the night hemisphere. We expect these cases to cover most undifferentiated bodies in the Solar System.

Discussion: The solar wind ram pressure supplies the magnetic energy at the dayside boundary of the body. If the body's conductivity is high enough to sufficiently stall the flow of wind, the magnetic pressure (hence amplification) is higher. For high β winds, the resulting mass loss perpendicular to the field lines and ram pressure increase, lowering the magnetic pressure. As per theory and observations, we expect Wind II (red) to be closest to the early solar wind. These simulation results are consistent with the wind parameter choices in [14].

Our results (Fig. 1) suggests that apart from the most resistive objects, all bodies can pile up magnetic fields. The effect is most pronounced for bodies with a conductive shell. But even the amplification ($A > 9$) in constant profile cases can explain the magnetizations found in some meteorites (e.g., CV3 meteorite Kaba). In these cases, the paleointensity of the meteorite together with ambient fields from our solar wind-induced magnetization models can also be used to constrain the orbital distance of the parent body at the time of magnetization, providing important constraints on Solar System evolution [3]. This methodology may be extended to other Solar System bodies, such as the Moon, for which an approximate resistivity structure and the maximum possible incident plasma or solar wind intensity are known. Solar wind-induced magnetizations may also help explain magnetizations observed in future space missions to asteroids, such as (16) Psyche, where the nature of the body [13,15] or presence/absence of a past core dynamo is unknown.

Acknowledgments: AA acknowledges a Horton Graduate Fellowship (UR Laboratory for Laser Energetics). The authors thank the UR Center for Integrated Research Computing for computational resources and technical support. Support was provided from NSF grants PHY-2020249, and EAR-2051550, and NASA grant 80NSSC19K0510.

References: [1] Scott E.R.D., Krot A.N. (2014), Chondrites and Their Components. Elsevier, *Oxford*, p. 6. [2] Carporzen L. et al. (2011), *Proc. Natl. Acad. Sci.*, 108, 6386. [3] O'Brien T. et al. (2020), *Commun. Earth Environ.*, 1, 1. [4] Fu, R.R., et al., (2021), *AGU Adv.*, 2, e2021AV000486. [5] Cournede C. et al. (2015) *Earth Planet. Sci. Lett.*, 410, 62. [6] Tarduno J.A. et al. (2017) *LPSC XLVIII*, Abstract #2850. [7] Anand A. et al. (2021), *MNRAS*, 509, 2957-2968. [8] Cunningham A. J. et al. (2009), *ApJS*, 182, 519. [9] Carroll-Nellenback J. et al., (2013), *J. Comput. Phys.*, 236, 461. [10] Johnstone C. et al. (2015), *A&A*, 577, A28. [11] Blackman E.G., Owen J.E. (2016), *MNRAS*, 458, 1548. [12] Tarduno J.A. et al. (2014), *Phys. Earth Planet. Inter.*, 233, 68. [13] Elkins-Tanton L. T. et al., 2020, *J. Geophys. Res.*, 125, e06296. [14] Oran R. et al. (2018), 2018, *Earth Planet. Sci. Lett.*, 492, 222. [15] Johnson B.C. et al. (2020), *Nat. Astron.*, 4, 41.